Atom-Resolved Noncontact Atomic Force Microscopic Observations of CeO_2(111) Surfaces with Different Oxidation States: Surface Structure and Behavior of Surface Oxygen Atoms

Yoshimichi Namai, Ken-ichi Fukui,† and Yasuhiro Iwasawa*

Department of Chemistry, Graduate School of Science, The University of Tokyo, 7-3-1 Hongo, Bunkyo-ku, Tokyo 113-0033, Japan

Received: January 31, 2003; In Final Form: July 7, 2003

Hexagonally arranged surface oxygen atoms, oxygen point defects, and multiple oxygen defects at oxygen-terminated CeO_2(111) surfaces in different oxidation states were visualized by noncontact atomic force microscopy (NC-AFM). The multiple defects such as line defects and triangular defects were stabilized by a local reconstruction, where edge oxygen atoms surrounding the multiple defects were displaced and gave enhanced brightness due to a geometric reason. Successive NC-AFM measurements of the same area of a slightly reduced CeO_2(111) surface revealed that hopping of surface oxygen atoms faced to metastable multiple defects was thermally activated even at room temperature. In contrast, no hopping was observed either at a point oxygen vacancy or a line defect that is stabilized by local reconstruction. It was also confirmed from atom-resolved NC-AFM observations that the surface oxygen defects were easily healed by exposure to O_2 gas at room temperature.

1. Introduction

Cerium oxides (CeO_{2-x}) have been used in a variety of industrial applications such as catalysis, fuel cells, and oxygen sensing, due to their high oxygen transport and storage capacities.[1−3] For example, cerium oxides show unique activities for various catalytic reactions such as oxidation of CO, removal of SO_x from fluid catalytic cracking (FCC) flue gases, oxidative coupling of methane, water gas shift reaction, etc.[2,4] Cerium oxides have been most widely used as an active component in three-way catalysts for automobile exhaust gas treatments, where cerium oxides are believed to play a crucial role as an "oxygen storage" component to control the oxygen concentration of catalyst surfaces.[3] Cerium oxides have also been used as slurry for chemical mechanical polishing (CMP). CMP is a wafer surface planarization technology applied in the manufacturing of ultrafine semiconductor devices, advanced ceramics (silicon nitride), and glass substrates. Although the detailed reaction mechanism for CMP is still unknown, an oxidation of a polishing substrate by CeO_{2-x} is suggested to be important during the polishing.[5,6] Despite the importance of the technological applications, few studies on cerium oxide single-crystal surfaces have been reported to date.

Oxygen diffusion and other transport properties of oxides such as electrical conduction are mainly determined by the presence, concentration, and mobility of lattice defects and are believed to play a key role in catalysis. Oxygen transport materials have long been used as oxidation and ammoxidation catalysts, for which purpose the material must be susceptible to rapid reduction by the reagent and reoxidation by the incorporation of gaseous oxygen in the lattice.[7,8] Ceria and ceria−zirconia as oxygen storage and release components in three-way catalysts have made evident that transport properties could play a key role in processes where the availability of oxidant from the gas phase is not constant. Since diffusion of oxygen anions is sufficiently fast, a continuous supply of oxygen from the bulk to the surface always keeps a constant oxygen concentration in active surface oxidation sites.[4] Therefore, dynamic behaviors of oxygen atoms on the CeO_x surface are very important. Oxidation states of cerium oxide surfaces have been studied by X-ray photoelectron spectroscopy (XPS), ultraviolet photoelectron spectroscopy (UPS), and high-resolution electron energy loss spectroscopy (HREELS).[9] However, direct observations of atomic-scale surface structures and behaviors of surface oxygen atoms of CeO_{2-x} in different oxidation states are required to understand the key properties of cerium oxides in the various applications.

Theoretical calculations showed that a (111) surface is the most stable surface among low-index planes of CeO_2.[10,11] CeO_2 at its stoichiometric composition is an electrically insulating f-transition metal oxide with a wide band gap of ca. 6 eV.[9] Oxygen deficiencies lead to the reduction of Ce^{4+} to Ce^{3+} and to occupation of the empty states left in the band gap.[9] Actually, surface structures of a reduced nonstoichiometric CeO_{2-x}(111) were investigated by scanning tunneling microscopy (STM) at room temperature (RT) with tunneling current as low as 10 pA or at elevated temperatures of 573−773 K to increase the electronic conductivity of the substrate.[12,13] Surface reconstructions on CeO_2(001) and CeO_2(110) were observed by STM.[14,15] Nevertheless, to study a structure change from stoichiometric composition of CeO_2, noncontact atomic force microscopy (NC-AFM) is more favorable to image atomically cerium oxide surfaces independent of the oxidation states. Since the first report of atom-resolved NC-AFM images of TiO_2(110)-(1 × 1) with oxygen point defects,[16] several atom-resolved images of oxide surfaces have been reported.[17] Besides, it has been shown that NC-AFM can be applied to monitor dynamic processes of atoms[18] and molecules[19] on surfaces.

In this study, we applied NC-AFM to atomic-scale observations of CeO_2(111) surfaces depending on their oxidation states.

* To whom correspondence should be addressed: E-mail: iwasawa@chem.s.u-tokyo.ac.jp. Fax: +81-3-5800-6892.

† Present address: Department of Chemistry, Graduate School of Science and Engineering, Tokyo Institute of Technology, Ookayama, Meguro-ku, Tokyo 152-8550, Japan.

10.1021/jp030142q CCC: $25.00
Published on Web 09/26/2003

Several kinds of multiple defects were observed by NC-AFM, and they were locally reconstructed for stabilization. Unexpected hopping of surface oxygen atoms around multiple defects at RT were observed by successive NC-AFM measurements. Reoxidation of slightly reduced CeO_2(111) surfaces was also examined, and it was confirmed that surface oxygen vacancies were easily healed by exposure to O_2 at RT.

2. Experimental Section

The experiments were performed in an ultrahigh vacuum (UHV) AFM (JEOL JAFM4500XT) equipped with an ion gun, low-energy electron diffraction (LEED) optics, and an XPS electron energy analyzer (VG Scientific CLAM2) with an Mg Kα X-ray source. The base pressure was 1.0×10^{-8} Pa. A polished CeO_2(111) sample of $5.5 \times 1.2 \times 0.95$ mm^3 (Commercial Crystal Laboratories) was cleaned by several cycles of Ar^+ ion sputtering (3 keV for 3 min) and UHV annealing at 1173 K for 60 s. After the cleaning procedure, the surface exhibited a (1×1) LEED pattern and no trace of impurities such as calcium, which is a possible contaminant in bulk CeO_2, were detected by XPS. The azimuth for the CeO_2(111) sample was determined by an X-ray diffraction (XRD) measurement (Rigaku ATX-G) after all of the experiments in this paper and indicated on each NC-AFM image. For NC-AFM measurements, stiff and conductive silicon cantilevers with $f_0 = 250-350$ kHz and $k = 20-30$ N m^{-1} (NT-MDT) were used as force sensors. Resonant frequency shift of the cantilever was detected by the FM method.[20] Since the cantilevers were used without Ar^+ ion sputtering, we assumed that most of the surface of the Si tip was initially covered with a native oxide layer. Topographic images were obtained by applying a voltage to the Z piezo to keep the negative frequency shift constant during scanning the surfaces. Bias voltage (V_s) was applied to the sample between -0.17 and -0.93 V to compensate the average contact potential between the tip and the sample during imaging the surface by NC-AFM.[21] All NC-AFM measurements were performed at RT. The amplitude of vibration of the cantilever was approximately 6 nm.

3. Results

Figure 1a shows a typical atom-resolved NC-AFM image of a nearly stoichiometric CeO_2(111) surface.[22] Hexagonally arranged bright spots with a constant separation of 0.38 ± 0.02 nm, which corresponds to the (1×1) unit cell of the bulk-terminated CeO_2(111) structure (Figure 1b), were resolved. Surface energy calculations have shown that an oxygen termination at the top of the O−Ce−O layer is more stable than a Ce-layer termination.[10,11] This is partly because the oxygen termination at the top of the neutral O−Ce−O layer forms no dipole moment perpendicular to the surface. Besides, the coordination number of exposed Ce^{4+} to O^{2-} reduces from 8 in the bulk to 7 at the O-terminated surface but 4 at the Ce-terminated surface. These results suggest that the surface observed in Figure 1a is oxygen-terminated, and each bright spot corresponds to an oxygen anion at the top layer. The results are also consistent with ion scattering spectroscopy measurements by Mullins et al.[23] for CeO_2(111) thin films grown on Ru(0001) and Ni(111), where they concluded 90% of the CeO_2-(111) surface was terminated by an oxygen layer at the top of the O−Ce−O layer. Measurements of the electronic structure of a variety of oxide surfaces have shown that predominant point defects that form when the samples are heated or exposed to ion beam under UHV are oxygen vacancies.[24] Surface oxygen point defects were observed as isolated dark depressions, and

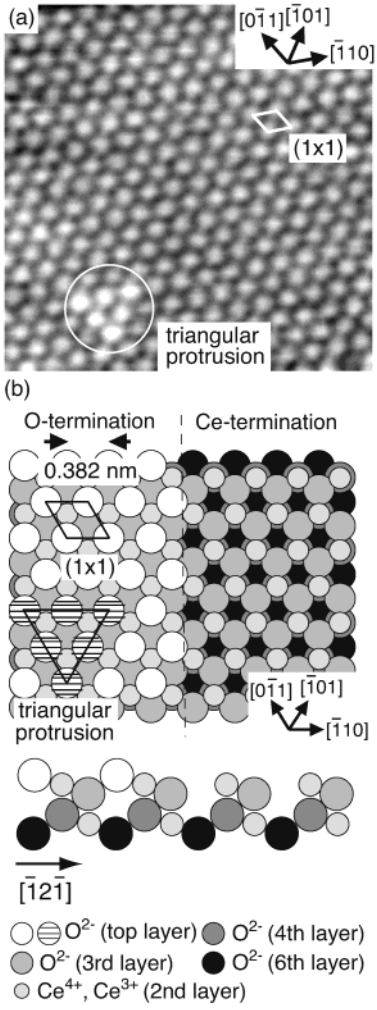

Figure 1. (a) Atom-resolved NC-AFM image (5.7×5.7 nm^2) of nearly stoichiometric CeO_2(111) surfaces. $\Delta f \sim 109$ Hz. (b) Model of the bulk-terminated structure of CeO_2(111) with oxygen-layer termination and cerium-layer termination. A triangular protrusion observed in (a) is also indicated on the model.

their density on the nearly stoichiometric surface was calculated to be $(0.8-1.7) \times 10^{12}$ cm^{-2} from the NC-AFM images obtained at different positions of the surface.[22]

In Figure 1a, a triangular protrusion enclosed by a circle was resolved into six bright spots whose apparent topographies were higher than other surface oxygen atoms by 0.03−0.05 nm but in-plane positions were almost identical to those expected for oxygen atoms on the bulk-terminated structure shown in Figure 1b. We observed several other equilateral triangular protrusions consisting of 6 or 10 oxygen atoms on nearly stoichiometric surfaces, and one of their apexes always pointed to the [$\bar{2}$11] direction. It is to be noted that such triangular protrusions were not observed on CeO_2(111) surfaces whose density of oxygen vacancies was higher than $(5.3-7.9) \times 10^{12}$ cm^{-2}.[22] Thus, the protruded structure may reflect local stress due to Coulomb repulsion between negatively charged oxygen anions, and the region with local stress may lead to formation of oxygen vacancies on the surface.

After the surface in Figure 1 was annealed at 1173 K for another 60 s, the density of surface oxygen vacancies increased to $(5.3-7.9) \times 10^{12}$ cm^{-2} (0.6−1.0% of top layer O^{2-}), but all of the oxygen defects observed were isolated point vacancies. In our experiments, multiple defects were not observed on CeO_2-(111) until the density of oxygen vacancies increased up to 1

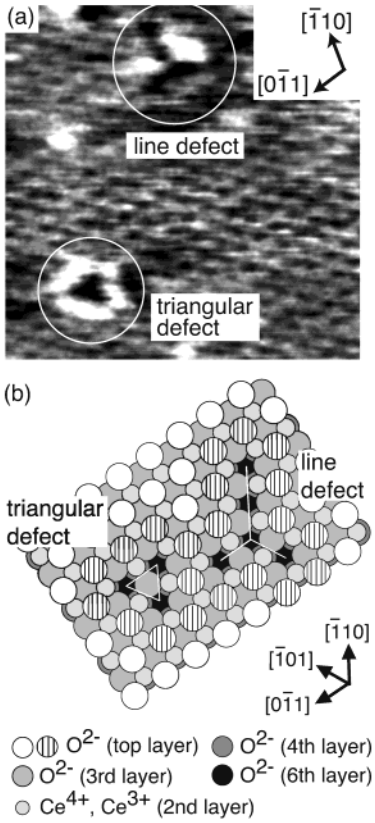

Figure 2. (a) NC-AFM image (5.7×5.7 nm^2) of a slightly reduced CeO_2(111) surface with multiple defects such as line defects and a triangular defect. $\Delta f \sim 258$ Hz. (b) Model of the line defect and the triangular defect observed in (a). Note that observed displacements for oxygen atoms surrounding the defects are not drawn in the model.

$\times 10^{13}$ cm^{-2}. By further increasing of the oxygen defect density to $(1.7-3.6) \times 10^{13}$ cm^{-2} (2.1−4.6% of top layer O^{2-}) by longer annealing of a CeO_2(111) surface at 1173 K for 4 min, multiple defects such as line defects and triangular defects formed as shown in Figure 2.[22] In contrast, oxygen point vacancies, which were exclusively observed by NC-AFM on the surfaces with an oxygen vacancy density less than 10^{13} cm^{-2}, became minor ones. Energy calculations for two oxygen point vacancies on CeO_2(111) indicated that association of two surface oxygen vacancies side by side was energetically favored against two isolated surface oxygen vacancies by 0.52 eV.[11] This partially explains why multiple defects are dominant at a higher density of oxygen defects. When the oxygen defect density is quite low, the entropy factor may overcome the energy factor during annealing at 1173 K. In this case, the point vacancy becomes dominant on the surface. Note that STM observations of CeO_2-(111) surfaces with a low density of oxygen vacancies are probably difficult due to lack of electric conductivity.[12,13]

Formation of Ce^{3+} by reduction leads to occupation of vacant 4f states within the band gap for stoichiometric CeO_2 as is evident from spectroscopy such as XPS[9,25] and EELS.[9] XPS spectra of partially reduced CeO_2 in the Ce 3d region can be well deconvoluted to peaks that are assignable to several final states (electronic configurations) of Ce^{4+} and Ce^{3+} without any apparent intermediate charge states.[9,25] In the elementary theory of defects in ionic solids, overall electroneutrality of the solid is preserved when defects are formed. Therefore, two excess electrons that were remained at O^{2-} vacancy by the unbalanced Coulomb potential probably reduce two Ce^{4+} cations to Ce^{3+} ions.

The multiple defects observed in Figure 2a qualitatively reproduced previous STM observations on nonstoichiometric CeO_{2-x}(111).[12,13] A triangular defect consisted of three neighboring oxygen vacancies and in-plane azimuth determination by XRD indicated that one apex of the triangular defect was pointed to the [2$\bar{1}\bar{1}$] direction. Therefore, the centroid of the triangular defect is a third layer oxygen atom (Figure 2b). In the oxygen-terminated (111) surface, a centroid of the triangle composed of three oxygen anions should be a cerium cation of the second layer or an oxygen anion of the third layer. If the cerium cation were at the centroid of the triangular defect directed to the [$\bar{2}$11] direction, the cation would have a bivalent Ce^{2+} that is energetically unfavorable.[12] This possibility was clearly denied by our experiments. The direction of the triangular defect was always rotated by 60° from the triangular protrusion in Figure 1a. It suggests a common driving force is responsible for formation of the two structures. Other than the triangular defect, line defects that consisted of oxygen vacancies from two to seven along the [$\bar{1}$10], the [$\bar{1}$01], and the [0$\bar{1}$1]directions were also observed (Figure 2b). In our observations, line defects were the major multiple defects on reduced CeO_{2-x}(111) surfaces and triangular defects were seldom observed. This is in contrast to STM observations by Nörenberg and Briggs, who observed triangular defects close to each other[12] or a hexagonally ordered multiple-vacancy structure whose component was assumed to be similar to the triangular defect.[13] The reason for the discrepancy is not clear at present but may be due to slightly different sample treatments.

Enhanced brightness at the edge oxygen atoms of triangular defects and line defects observed in the previous STM studies on CeO_2(111) was also observed by NC-AFM (Figure 2a). As revealed by the brighter contrast, they were higher in topography than oxygen atoms far from the line defect by 0.05−0.08 nm, slightly larger than the height difference of 0.03 nm reported by STM observations.[12] On the basis of the conventional view of reduction of two Ce^{4+} to two Ce^{3+} accompanied by an oxygen vacancy formation, six exposed Ce cations at the triangular defect and most of Ce cations exposed at the line defect ($2n$ of $(2n + 1)$ Ce cations for n-atom oxygen vacancies) are expected to be Ce^{3+}. Nörenberg and Briggs attributed the enhanced brightness at the edge oxygen to delocalization of electrons, which are otherwise supposed to be localized at Ce cations, to the surrounding oxygen anions.[12]

By extensive measurements of the line defects on CeO_2(111) with atomic-scale resolution by NC-AFM, we observed two types of line defects as shown in Figure 3a,b. In Figure 3a, both sides of oxygen atoms surrounding the line defect were observed with brighter contrast and besides they were displaced toward the defect. Their in-plane positions are schematically shown in a model of Figure 3c, where only the first layer oxygen anions are displaced. In Figure 3b, oxygen atoms at only the right-hand side of the line defect were observed with brighter contrast and displaced toward the defect by 0.05 nm. In contrast, oxygen atoms at the left-hand side were neither displaced nor imaged with a brighter contrast. Note that it is not an artifact, for example, by delayed feedback during measurements because a point oxygen vacancy was observed without enhanced contrast around it at the bottom left in Figure 3b. We have also observed multiple defects without a local reconstruction as will be shown later. At the triangular defect, which was a minor multiple defect in our observations on slightly reduced CeO_2(111) surfaces, oxygen atoms surrounding the defect showed enhanced contrast as clearly shown in Figure 2a and distorted toward the defect by 0.03−0.05 nm. These results of atom-displacement are

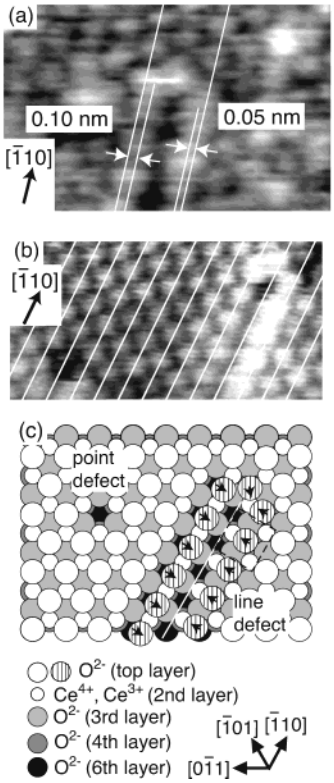

Figure 3. (a) NC-AFM image (3.5×2.3 nm^2) at a line defect observed on the same surface as Figure 2a. $\Delta f \sim 228$ Hz. (b) High-resolution NC-AFM image (4.5×2.0 nm^2) including a point defect and a line defect observed on the same surface as (a). $\Delta f \sim 171$ Hz. (c) Tentative model showing displacement of oxygen atoms surrounding the line defect observed in (a).

inconsistent to the previous view that redistribution of electrons around the multiple defects is the reason for brighter contrast around multiple defects.[12] We consider that displacement of oxygen atoms in the (111) plane is the major reason for the brighter contrast.

From successive measurements of the same area of CeO_2-(111) surfaces with different density of oxygen vacancies by NC-AFM, it was observed that some oxygen atoms hop to the neighboring oxygen vacancy sites on a slightly reduced surface with nonreconstructed multiple oxygen defects even at RT. Figure 4 shows such an example, where the oxygen defect density was $(1.8-2.0) \times 10^{13}$ cm^{-2}. Three neighboring oxygen atoms marked with circles in Figure 4c disappeared from those positions at the next frame in Figure 4d measured at an interval of 91 s, and instead two oxygen atoms were observed at the positions of oxygen vacancies observed in Figure 4c. The results suggest that oxygen atoms hopped to the neighboring sites in 91 s. The remaining third oxygen atom was probably hopping during scanning of Figure 4d between the three vacancies marked with gray circles as suggested by fragmented white traces observed at the vacancies. It should have been observed as an atom with normal shape at faster scanning speed which was not possible without degrading the image quality in our present system. Figure 5a,b also shows NC-AFM images of the same area of a slightly reduced CeO_2(111) surface with multiple defects observed at an interval of 182 s. The position of an oxygen vacancy changed in the multiple defect region M. Thus, oxygen atoms around multiple defects hop to the neighboring site at RT. Point defects marked as P in Figure 5 did not change in 182 s. Again, positions of oxygen point vacancies on CeO_2-(111) surfaces with low density of oxygen vacancies ($(1.2-6.6) \times 10^{12}$ cm^{-2}) did not change for more than 800 s. This

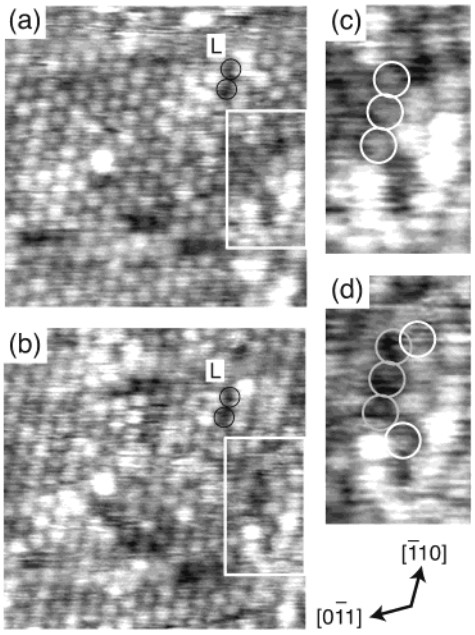

Figure 4. (a, b) Successive NC-AFM images of the same area of a slightly reduced CeO_2(111) surface with multiple defects observed at RT. Site changes of some surface oxygen atoms occurred between 91 s taken for scanning the whole area of 10.3×10.3 nm^2. The image size shown here is 5.8×5.8 nm^2. $\Delta f \sim 171$ Hz. (c) and (d) are magnified images of the square area (1.5×2.6 nm^2) in (a) and (b), respectively. Oxygen atoms changed their positions between (c) and (d) as indicated by white circles. Positions of the white circles in (c) are indicated as gray circles in (d) for a guide. L denotes a double defect with displaced oxygen atoms with brighter contrast.

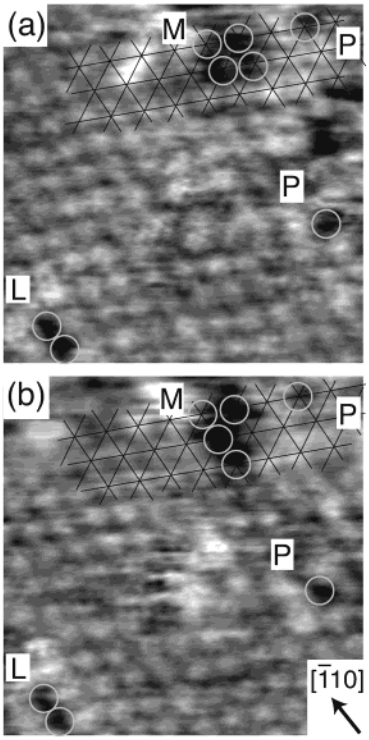

Figure 5. (a, b) Successive NC-AFM images (4.18×4.18 nm^2) of the same area of a slightly reduced CeO_2(111) surface with multiple defects observed at RT. $\Delta f \sim 263$ Hz. Time intervals for obtaining (a) and (b) were 182 s. M and P are multiple and point oxygen vacancies. L denotes a line defect with displaced oxygen atoms with brighter contrast.

indicates that hopping of oxygen atoms around point defects may be negligible and particularby hopping of oxygen atoms

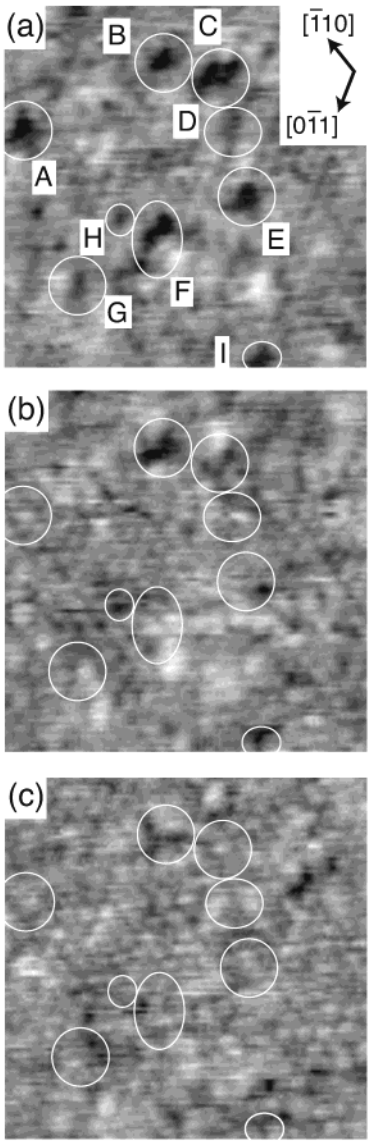

Figure 6. Successive NC-AFM images (7.5 × 7.5 nm^2) of the same area of a slightly reduced CeO_2(111) surface with multiple defects under oxygen exposure at RT. $\Delta f \sim 437$ Hz. Some multiple defects and point defects were healed by oxygen atoms between 91 s taken for scanning the whole area of 10.3 × 10.3 nm^2. The same positions were indicated by white circles for a guide.

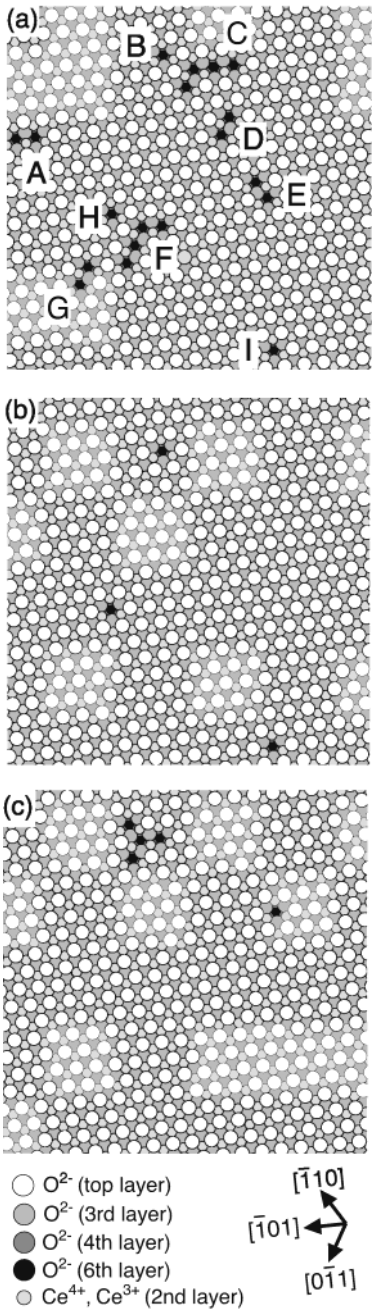

Figure 7. Positions of oxygen vacancy sites observed in Figure 6a−c.

on the surface without multiple defects is not activated at RT. Further, multiple oxygen vacacies at reconstructed sites (marked as L in Figure 5) were stable, where no structure change were observed at RT.

Reoxidation of slightly reduced CeO_2(111) surfaces were also examined. Figure 6 shows NC-AFM images before and after exposure of a slightly reduced CeO_2(111) surface to O_2 gas at RT. Dark regions in Figure 6a are multiple oxygen vacancies without local reconstruction. Location of oxygen vacancy sites is illustrated in Figure 7. Exposure to O_2 gas healed the multiple oxygen vacancies; the healed sites showed bright spots with the (1 × 1) periodicity, and contrasts similar to those for surrounding oxygen atoms were observed in Figure 6b,c. Thus, O_2 molecules dissociate to oxygen atoms at the multiple oxygen vacancies and the produced oxygen atoms heal the vacancies at RT. The result strongly supports our assignment that bright spots observed by NC-AFM corresponds to oxygen atoms and a nearly stoichiometric CeO_2(111) surface is O-terminated. There are also minor point vacancies on the surfaces in Figure 6a. The oxygen point vacancies were not healed by O_2 exposure for 91 s, but some of them were healed after 273 s under the O_2 ambient (Figure 6c and Figure 7c). Readsorption of oxygen on the point defects is much slower than that on the multiple defects.

4. Discussion

4.1. Oxygen Defect Structures of the CeO_2(111) Surface. Energy calculations of an oxygen point vacancy and two accompanying Ce^{3+} at different positions in the bulk and at low-index planes of CeO_2 indicated that the oxygen vacancy preferred the surfaces to the bulk and two Ce^{3+} occupied exposed surface sites associated with the oxygen vacancy.[10,11] Besides, association of two surface oxygen vacancies side by side on CeO_2(111) was calculated to be energetically favored against two isolated surface oxygen vacancies by 0.52 eV.[11]

These calculations included Coulomb interaction, short-range interaction consisting of Born repulsion and attractive van der Waals interaction, and polarization interaction based on the shell model, and neither displacement nor relaxation of atoms at vacancy sites was considered.[10,11] Reasons for the lowering of the energy by association of two defects were not clearly stated, but perhaps an occupation of a second-layer site in contact with two neighboring oxygen vacancies by Ce^{3+} is favored.[11] In our experiments, however, multiple defects were not observed on CeO_2(111) until the density of oxygen vacancies increased up to 1×10^{13} cm^{-2}, and at the defect density of $(1.7-3.6) \times 10^{13}$ cm^{-2} (2.1−4.6% of top layer O^{2-}), multiple defects such as line defects and triangular defects were dominantly observed. If the oxygen defect density is quite low, the entropy factor may overcome the energy factor during annealing at 1173 K and then the point vacancy becomes dominant on the surface. Another factor we have to mind is that surfaces we observed by NC-AFM may be somewhat in nonequilibrium because they were quenched from 1173 K to RT.

Multiple defects such as line defects and triangular defects formed at the higher oxygen defect density of $(1.7-3.6) \times 10^{13}$ cm^{-2} (2.1−4.6% of top layer O^{2-}). As shown in Figures 2a and 3, enhanced brightness at the edge oxygen atoms of triangular defects and line defects was often observed. Such enhanced brightness was also observed in a previous STM study by Nörenberg and Briggs, and they attributed the enhanced brightness at the edge oxygen to delocalization of electrons, which are otherwise supposed to be localized at Ce cations, to the surrounding oxygen anions.[12] If redistribution of electrons to the oxygen atoms faced to the multiple defects occurs, different charge density on oxygen anions should affect the interaction between the tip and the sample, which leads to a different contrast on the NC-AFM images as shown by recent NC-AFM experiments and theoretical calculations.[17] However, enhanced brightness around the line defect was always accompanied by in-plane displacement of the oxygen atoms in our observations as mentioned above. If we simply assume that the amount of electrons redistributed to each edge oxygen atoms surrounding the multiple defects is inverse by proportional to the number of the oxygen atoms per an oxygen vacancy (or per a released electron), it should have an order of the following: a point vacancy < a line defect with a few vacancies < a triangular defect with three vacancies < a line defect with more than five vacancies. Such a tendency was not observed in the present NC-AFM measurements on oxygen defects on CeO_2-(111).

From our NC-AFM observations, we consider that the displacement of oxygen atoms in the (111) plane is the major reason for the brighter contrast. If we simply postulate that only the first layer oxygen atoms with brighter contrast in Figure 3a are displaced from the bulk-terminated positions, while fixing the distance to exposed Ce cations to 0.234 nm, which is the distance between the O atom and the Ce atom in the bulk, oxygen atoms on the left-hand side and the right-hand side of the line defect will be lifted up by 0.06 and 0.08 nm, respectively. These values are similar to those observed by NC-AFM. However, if the displacement is caused by a relaxation of the first layer oxygen to compensate the repulsion between oxygen anions at the first layer, a question remains why the second-nearest oxygen atoms from the line defects were not displaced. Each Ce^{4+} cation in bulk CeO_2 has eight equivalent oxygen anions separated by 0.234 nm. In bulk Ce_2O_3, which is another stoichiometric phase with Ce^{3+} cations, each Ce^{3+} cation is coordinated with seven oxygen anions separated by 0.234 nm (three), 0.243 nm (one), and 0.270 nm (three), respectively. Thus, reduction of Ce^{4+} to Ce^{3+} may lead to local expansion. Volume expansion according to the reduction of CeO_2 was actually observed, and it was attributed to larger ion diameter of Ce^{3+} than Ce^{4+}.[1,4] Hence local displacement including the second and third layer atoms at the line defect may occur, but NC-AFM observations cannot make this sort of conclusion. The other type of line defects shown in Figure 3b may be a metastable phase, which should be converted to the defect type in Figure 3a. Bevan[26] has reported that a type-C bcc structure (cubic bixbyite structure) formed between $CeO_{1.69}$ and $CeO_{1.65}$ by XRD measurements when CeO_2 was reduced in hydrogen to varying degrees. Cubic bixbyite structure[27] is known as a stable phase for Pr_2O_3, which is sesquioxide of PrO_2 with a cubic fluorite structure. The cubic bixbyite structure of Pr_2O_3 is closely related to the PrO_2 structure.[28] Its unit cell consists of 8 unit cells of PrO_2 in which 16 oxygen atoms have been removed in a regular way. Due to these vacancies, 24 among 32 Pr atoms in the unit cell are shifted slightly from the positions they formerly occupied in the PrO_2 structure. The 48 oxygen atoms are also slightly distorted from the PrO_2 position. There is a similarity between local arrangement of atom positions of the (110) face of cubic bixbyite structure and the region surrounded by a rectangle in Figure 3c. The line defect observed in Figure 3b is similar to the (110) face of a cubic bixbyite structure. Local reconstruction at this region and that at the three sides of triangular defects are considered to be identical. In Figure 3a, a right side of the multiple defect is similar to the (110) face of cubic bixbyite structure but a left side of the multiple defect is different from the (110) face of cubic bixbyite structure. The cubic bixbyite structure is very complicated. In a region with a structure similar to that the (110) face of cubic bixbyite structure, atom positions in two-dimensional direction of first layer oxygen atoms and third layer oxygen atoms have a similarity to the (110) face of cubic bixbyite structure. The part of the oxygen atoms in the multiple defects, which has the similarity to the cubic bixbyite structure, was similar to the (110) face of the cubic bixbyite structure in three-dimensional direction. However, the atom positions of the Ce cation had only a few similarities to those of the (110) face of cubic bixbyite structure. Thus, the part of local reconstruction may relate to the local transformation to cubic bixbyite structure. The major contribution of the geometry of constituent atoms to imaging of a reconstructed CeO_2(001) surface by STM was confirmed by comparison with a theoretical calculation.[15] Our preliminary STM measurements of multiple defects on nonstoichiometric CeO_{2-x}(111) also indicated that the enhanced brightness around the multiple defects was always accompanied by in-plane displacement of edge oxygen atoms.

4.2. Hopping of Surface Oxygen Atoms on Reduced CeO_2-(111) Surfaces. CeO_2 is known as a prominent material for its high oxygen storage capacity depending on the oxidation states and used as a component of catalysts as mentioned above. Diffusion coefficients and diffusion activation energies for oxygen atoms in bulk CeO_{2-x} have been estimated by gas-phase analysis during the exchange reaction of $^{18}O_2$ with bulk ^{16}O above 1000 K by a mass spectrometer[29] or by the depth profile analysis of the concentration of ^{18}O after the exchange reaction by secondary ion mass spectrometry (SIMS).[30] A diffusion coefficient of stoichiometric CeO_2 was rather high among various oxides, and the value became higher for reduced CeO_{2-x}.[1,29] Besides, the activation energy of oxygen diffusion in CeO_{2-x} bulk measured at 1200−1400 K decreased from 104 kJ mol^{-1} for nearly stoichiometric CeO_2 to 15 kJ mol^{-1} for

$CeO_{1.80}$.[29] A recent static SIMS study on self-diffusion in nearly stoichiometric CeO_2 using labeled oxygen and cerium showed that surface oxygen atoms began to exchange with the bulk oxygen around 550 K, while Ce cations were immobile up to 900 K.[31] Thus, hopping of surface oxygen atoms on CeO_2(111) at RT observed in Figures 4 and 5 may be unexpected from the conventional view. Quite recently, Schaub et al.[32] proposed an adsorbate-mediated diffusion mechanism for surface oxygen vacancies on TiO_2(110) on the basis of their successive STM observations at high speed on atomic-scale resolution. While the surface oxygen vacancies were not mobile at RT under UHV condition, they became mobile after exposure to O_2 at RT. They proposed that the migration of oxygen vacancies occurred by transiently adsorbed molecular oxygen; an adsorbed oxygen molecule dissociates at an oxygen point defect and forms an oxygen adatom, and then this adatom with high reactivity recombines with a surface oxygen atom to form an O_2 molecule, resulting in oxygen defect movement as a net process. Tanner et al.[33] have observed by successive STM observations that the oxygen atoms of the topmost layer on WO_3(001)-$c(2 \times 2)$ surface are mobile even at room temperature. Although the origin for rapid movement was not clearly stated, it may relate with the layer's open structure that half a monolayer of terminal oxygen covers the WO_2 plane.

Hopping of surface atoms or adsorbed molecules may be sometimes induced or at least accelerated by a scanning tip during SPM measurements. A scanning tip on a cantilever traces the surface while vibrating at a determined frequency adjusted by changing the distance from the surface using the feedback loop. Hopping directions of two oxygen atoms from Figure 4c to Figure 4d are $+15°$ (at point vacancy) and $-48°$ (at double vacancies) from the fast-scanning direction of the horizontal line, respectively. Taking into consideration other images independently observed, the hopping around point defects was a minor event. The hopping of oxygen atoms at the multiple oxygen vacancies in Figures 4 and 5 was always observed as a major event. The hopping direction did not have a strong correlation with the fast scanning direction. On a little more reduced CeO_2(111) (7.3−9.1% of oxygen vacancies that were mostly line defects), we have performed preliminary experiments of successive STM observations at an interval of 91 s/flame at RT and 350 and 400 K, respectively. We can only roughly analyze the temperature dependency because of poor time resolution limited by the minimum tunneling current applicable in our STM system. The STM image itself had poorer spatial resolution than NC-AFM (not shown here), but measurements at elevated temperature were easier than those for NC-AFM due to technical reasons. By comparing two successive flames at an interval of 91 s, we have calculated the minimum path length for oxygen atoms to reproduce the oxygen positions in the latter frame by assuming that oxygen atoms can only hop to the neighbor vacancies. And the value was averaged over the oxygen atoms (typically 43 hopping events at 400 K) and plotted versus T^{-1}. Although the value of the minimum path length is probably deviated from the real value particular at higher temperature due to the poor time resolution, we have calculated the apparent activation energy from the slope by assuming that the minimum path length has Arrhenius-type behavior (Arrhenius plot). The value was estimated to be about 30 kJ $mo1^{-1}$ with an energy of 15 kJ $mo1^{-1}$. These results suggest that the hopping of oxygen on CeO_2(111) is a thermal process activated even at room temperature and not strongly affected by a scanning tip.

No apparent change in the displaced oxygen atoms denoted as L in brighter contrasts around the line defect on CeO_2(111) in Figures 4 and 5 was observed by successive NC-AFM measurements. This is consistent with stable imaging of the line defect structures by NC-AFM as shown in Figure 3a,b. It is also consistent with our assumption that the multiple defects are stabilized by local reconstruction. Thus, the hopping of oxygen atoms observed at RT occurs preferentially at metastable multiple defect structures which could not complete the local reconstruction during quenching from annealing temperature of 1173 K to RT. The driving force of the hopping is probably repulsion between the first layer of oxygen anions. Hopping of an oxygen atom heals a neighboring oxygen vacancy while forming a new vacancy at the originally occupied site. If multiple defects without any local reconstruction are energetically favored against isolated oxygen point vacancies as suggested by an energy calculation,[11] multiple defects remain on the surface without spreading into pieces by the hopping events.

Our NC-AFM observations showed that the hopping event was negligible at an oxygen point vacancy on CeO_2(111) at RT. If negatively charged oxygen atoms were postulated at an intermediate position in a hopping event and only Coulomb interaction is taken into consideration, multiple defects are energetically preferred to point vacancies due to less repulsion. To compensate local charge and maintain the driving force, a hopping oxygen may be a neutral atom that gives two electrons to two coordinated Ce^{4+} and receives two electrons from two Ce^{3+} facing the original vacancy. The former process is similar to the formation of an oxygen vacancy by a thermal process. If such processes are the key issues, the different activation between multiple defects and a point vacancy may not be explained. There should be another factor to control the oxygen hopping event.

4.3. Facile Reoxidation of Slightly Reduced CeO_2(111) Surfaces. Exposure of a slightly reduced CeO_2(111) surface to O_2 gas at RT healed the oxygen vacancies as shown in Figures 6 and 7. This is consistent with previous XPS and EELS studies.[9,25] The oxygen sticking probability at the oxygen vacancy sites was estimated to be 0.04 by the serial NC-AFM observation. Although we could not obtain any information of reoxidation of subsurface oxygen vacancies by NC-AFM images, surface oxygen vacancies were healed and the oxygen atoms occupied bulk-terminated positions with contrast similar to that of a stoichiometric surface observed in Figure 1. From a different point of view, this result is proof that the nearly stoichiometric CeO_2(111) surface is O-terminated and each bright spot observed by NC-AFM corresponds to a surface oxygen atom. If the (111) surface was cerium-terminated and if NC-AFM imaged each cerium atom, the same position as the cerium vacancy could not be healed by oxygen because the cerium vacancy site is composed of only oxygen anions as shown in Figure 1b. A higher temperature such as 550 K is probably needed for reoxidation of bulk oxygen vacancies on the basis of the SIMS study.[31] In this study, facile reoxidation of the CeO_2 surface was confirmed on the atomic scale. This is the first step of understanding of the facile oxidation−reduction processes occurring on CeO_{2-x} in the working states in chemical processes such as catalysis.

5. Conclusions

Structures of CeO_2(111) surfaces and behavior of the surface oxygen atoms at different oxidation states were studied by atom-resolved NC-AFM observations. Atom-resolved NC-AFM images indicated that there were several types of the line defects

but edge oxygen atoms with enhanced brightness were always displaced from the bulk-terminated positions. It was concluded that such multiple defects were locally reconstructed for stabilization that resulted in enhanced brightness of edge oxygen atoms. Successive NC-AFM measurements revealed that hopping of surface oxygen atoms to neighboring vacant sites occurred at metastable multiple defects without enhanced brightness even at RT. It was a thermally activated process that occurred even at RT and was accelerated at higher temperatures. It was confirmed that surface oxygen defects can be easily healed by O_2 exposure at RT. Accumulated knowledge on mobility of surface oxygen atoms by direct observations using NC-AFM will elucidate dynamic surface events of CeO_{2-x} with its facile oxidation−reduction property which is relevant to a variety of applications to catalysis.

Acknowledgment. This study was supported by a Grant-in-Aid for The 21st Century COE Program for Frontiers in Fundamental Chemistry from the Ministry of Education, Culture, Sports, Science, and Technology. We thank Prof. A. Kobayashi and the Rigaku Corp. X-ray Research Laboratory for help to measure the XRD of a CeO_2(111) sample to determine the in-plane azimuth.

References and Notes

(1) Mogensen, M.; Sammes, N. M.; Tompsett, G. A. *Solid State Ionics* **2000**, *129*, 63.
(2) Trovarelli, A. *Catal. Rev.−Sci. Eng.* **1996**, *38*, 439.
(3) Yao, H. C.; Yao, Y. F. Y. *J. Catal.* **1984**, *86*, 254.
(4) Trovarelli, A., Ed. *Catalysis by ceria and related Materials*; Imperial College Press: London, 2002.
(5) Cook, L. M. *J. Non-Cryst. Solids* **1990**, *120*, 152.
(6) Jiang, M.; Komanduri, R. *Key Eng. Mater.* **2001**, *202−203*, 1.
(7) Mazanec, T. J. *Solid State Ionics* **1994**, *70−71*, 11.
(8) Gellings, P. J.; Bouwmeester, H. J. M. *Catal. Today* **1992**, *12*, 1.
(9) Pfau, A.; Schierbaum, K. D. *Surf. Sci.* **1994**, *321*, 71.
(10) Sayle, T. X. T.; Parker, S. C.; Catlow, C. R. A. *Surf. Sci.* **1994**, *316*, 329.
(11) Conesa, J. C. *Surf. Sci.* **1995**, *339*, 337.
(12) Nörenberg, H.; Briggs, G. A. D. *Phys. Rev. Lett.* **1997**, *79*, 4222.
(13) Nörenberg, H.; Briggs, G. A. D. *Surf. Sci.* **1999**, *424*, L352.
(14) Nörenberg, H.; Briggs, G. A. D. *Surf. Sci.* **1999**, *433−435*, 127.
(15) Nörenberg, H.; Briggs, G. A. D. *Surf. Sci.* **2001**, *477*, 17.
(16) Fukui, K.; Onishi, H.; Iwasawa, Y. *Phys. Rev. Lett.* **1997**, *79*, 4202.
(17) Morita, S., Wiesendanger, R., Meyer, E., Eds. *Noncontact Atomic Force Microscopy*; Springer: New York, 2002.
(18) Sugawara, Y.; Ohta, M.; Ueyama, H.; Morita, S. *Science* **1995**, *270*, 1646.
(19) Fukui, K.; Iwasawa, Y. *Surf. Sci.* **2000**, *464*, L719.
(20) Alberecht, T. R.; Grütter, P.; Horne, D.; Rugar, D. *J. Appl. Phys.* **1991**, *69*, 668.
(21) Howald, L.; Lüthi, R.; Meyer, E.; Güntherodt, H. J. *Phys. Rev. B: Condens. Matter Mater. Phys.* **1995**, *51*, 5484.
(22) Fukui, K.; Namai, Y.; Iwasawa, Y. *Appl. Surf. Sci.* **2002**, *188*, 252.
(23) Mullins, D. R.; Radulovic, P. V.; Overbury, S. H. *Surf. Sci.* **1999**, *429*, 186.
(24) Henrich, V. E., Cox, P. A., Eds. *The surface science of metal oxides*; Cambridge University Press: Cambridge, U.K., 1994.
(25) Romeo, M.; Bak, K.; Fallah, J. E.; Normand, F. L.; Hilaire, L. *Surf. Interface Anal.* **1993**, *20*, 508.
(26) Bevan, D. J. M. *J. Inorg. Nuclear Chem.* **1955**, *1*, 49.
(27) Wyckoff, R. W. G. *Crystal Structures*; Interscience: New York, 1963−1971.
(28) Eyring, L.; Baenziger, N. C. *J. Appl. Phys.* **1962**, *33*, 428.
(29) Floyd, J. M. *Indian J. Technol.* **1973**, *11*, 589.
(30) Kamiya, M.; Shimada, E.; Ikuma, Y.; Komatsu, M.; Haneda, H. *J. Electrochem. Soc.* **2000**, *147*, 1222.
(31) Perkins, C. L.; Henderson, M. A.; Peden, C. H. F.; Herman, G. S. *J. Vac. Sci. Technol., A* **2001**, *19*, 1942.
(32) Schaub, R.; Wahlström, E.; Rønnau, A.; Lægsgaard, E.; Stensgaard, I.; Besenbacher, F. *Science* **2003**, *299*, 377.
(33) Tanner, R. E.; Meethunkji, P.; Altman, E. I. *J. Phys. Chem. B* **2000**, *104*, 12315.